IEEE Access
Multidisciplinary | Rapid Review | Open Access Journal

Received February 6, 2020, accepted March 2, 2020, date of publication March 9, 2020, date of current version March 19, 2020.

Digital Object Identifier 10.1109/ACCESS.2020.2979172

3-Wavelength (UV, Blue, Red) Controlled Photo-Confinement for 3D-Printing: Kinetics and Modeling

JUI-TENG LIN[1], HSIA-WEI LIU[2], YIN-CHEN CHIU[3], KUO-TI CHEN[3], AND DA-CHUAN CHENG[4]

[1]Photon Vision Corp., Taipei 114, Taiwan
[2]Department of Life Science, Fu Jen Catholic University, New Taipei City 242, Taiwan
[3]Graduate Institute of Applied Science and Engineering, Fu Jen Catholic University, New Taipei City 242, Taiwan
[4]Department of Biomedical Imaging and Radiological Science, China Medical University, Taichung 404, Taiwan

Corresponding author: Da-Chuan Cheng (dccheng@mail.cmu.edu.tw)

This work was supported in part by China Medical University, Taiwan, under Grant CMU 108-S-25.

ABSTRACT Detailed kinetics for a 3-wavelength photopolymerization confinement (PC) system is presented for both numerical solutions and analytic formulas. The dynamic profiles of oxygen, free radicals, and monomer conversion for various situations of: blue-light only, 2-light (red and UV), and 3-light (red, blue, UV) are obtained. Higher oxygen concentration leads to a lower conversion, which could be enhanced by reducing the S-inhibition via a red or blue light pre-irradiation. We found that pre-irradiation time is given by TP = 200 s for red-light only, and reduced to 150 s, for both red and blue-light. The system under UV-only leads to a conversion lower than that of blue-only. However, conversion could be improved by the dual-light (blue and UV), and further enhanced by the pre-irradiation of red-light. The two competing factors, N-inhibition and S-inhibition, could be independently and selectively tailored to achieve: (i) high conversion of blue-light (without UV-light), enhanced by red-light pre-irradiation for minimal S-inhibition; and (ii) efficient PC initiated by UV-light produced N-inhibition for reduced confinement thickness and for high print speed.

INDEX TERMS Kinetic model, photopolymerization, additive manufacturing, 3D printing.

I. INTRODUCTION

Various methods and materials for 3D printing and customized additive manufacturing (AM) have been reported [1]–[3]. Except nonmetal printing technique, there are also some other metal 3D printing methods, such as selective laser melting [4]–[6]. Conventional photolithographic rapid prototyping is limited to a very thin layer of photo cured material having strong absorbing at a specific wavelength. Contemporary stereo lithographic devices use a single wavelength light to initiate polymerization patterned in a plane. However, the single-wavelength irradiation suffers the loss of polymerization confinement by accumulation of non-target light exposure [3], [7]. To overcome this drawback, two-color (UV and blue light), direct-write photolithography was reported, in which the UV-light polymerization inhibition is concurrent with the blue-light orthogonal, patterned photopolymerization [8]–[10].

The associate editor coordinating the review of this manuscript and approving it for publication was Chi-Tsun Cheng.

Photopolymerization confinement (PC) is one of the key methods for AM system for continuous printing at relatively high linear velocities, in addition to printing 3D structures using a single exposure [9], [10]. PC is defined by the balance point (in space) of initiation and inhibition, such that uncured resin is confined in a boundary immediately adjacent to the glass window, eliminating adhesion and enabling continuous operation of 3D printing. An ideal AM system for efficient PC using a 3-wavelength (UV, red and/or blue light) requires the following conditions: (i) the photoinhibition light (UV) must yield significantly cease polymerization, while keeping sufficiently high polymerization rates produced by the initiation light (blue or red); (ii) a wide range of compatible monomers and co-initiators; (iii) the photoinhibition of free-radical chain-growth can be rapidly switched on and off by cycling the UV light; (iv) the formulated resins can be spatially confined using concurrent blue and UV irradiation; (v) rapid elimination of the inhibitor species in the dark, or after cessation of UV exposure; (vi) large polymerization inhibition depth adjacent to the projection window; and

(vii) continuous part production at translation speeds of several hundred millimeters per hour. Above idea conditions allow for rapid, single-exposure fabrication of complex structures which cannot be easily achieved by conventional single-wavelength methods.

Previously reported inhibition layers via oxygen inhibition are typically only tens of micrometers thick, and thus it requires the use of low-viscosity resins or fabrication of objects with small cross sections [3], [7]. Single-wavelength, conventional and diffusion-reliant methods with a large inhibition thickness (IT) and high photoinitiation rates offer a continuous and rapid object printing [8], [9]. However, they suffer the issues of separation resin reflow. In dual-wavelength systems, the IT may be reduced by decreasing irradiation intensity and thus increase the print speeds as polymerization proceeds closer to the projection window. For a given resin composition, the IT depends on the ratio of inhibitor to initiator absorbance, quantum yield of the radicals, reaction rates among the radicals and monomers, initiator, co-initiator and inhibitor, and the light intensity and dose (or exposure time).

Dual-wavelength PC were reported in both parallel and perpendicular concurrent irradiation schemes [9], [10]. Volumetric PC was achieved by inhibition depth controlled by varying the ratio UV and blue lights intensity, where print speeds of 2 m/hour have been achieved in a wide variety of resins including acrylates, methacrylates, and vinyl ethers [9]. In addition, by varying the intensity of the light source on a per-pixel basis, the system can perform surface topographical patterning in a single exposure layer with no stage translation. In the perpendicular scheme, photopolymerizations were reported to confine in depth the regional polymerized resin, in which two perpendicular blue and UV lights, independently effect polymerization initiation and inhibition, respectively [10].

As reported by van der Laan *et al.* [10], the effectiveness of a photoinhibitor is strongly monomer-dependent, and requires: (i) a high conversion of blue-photoinitiation in the absence of the UV-active inhibitor; (ii) a strong chain termination with significant reduction of blue and UV conversion in the presence of UV-active inhibitor; and (iii) short induction time or rapid elimination of the inhibitor species in the dark (or absence of UV-light), such that the initiation-inhibition cycles may be switched on and off rapidly. Moreover, a short induction time may be achieved by high UV intensity or large inhibitor-concentration, and it also requires minimum impurity and oxygen which cause a delayed curing of the resin.

The monomer-dependence of a dual-wavelength PC was reported by van der Laan *et al.* [10], in which different monomers have different C=C bond rate constants (K) under the exposure of blue, UV and blue+UV. For example, bisphenol ethoxylate diacrylate (BPAEDA) resins formulated with camphorquinone (CQ) and ethyl 4-(dimethylamino)benzoate (EDAB), for 0% butyl nitrite (BN), have a maximum conversion rate constant Kmax= 0.675 (1/s) (at blue+UV), which is reduced to 0.0106 (for 1%BN). Therefore, BPAEDA is a better candidate than trimethylolpropane triacrylate (TMPTA) which only has a 3 times reduction of Kmax.

We have previously reported the kinetics and modeling of a single-wavelength radical-mediated photopolymerization in single-initiator [11]–[13], two-initiator [14], and two-component systems [15]. We also introduced a new criterion for an effective PC based on a dual-wavelength (UV and blue) system, in which the UV-light serves as an inhibition for PC, named as N-inhibition. We have further reported a dual-wavelength (UV and red), in which the red-light serves as a reduction of singlet-oxygen inhibition, named as S-inhibition [16]. This study will extend our previous modeling to a 3-wavelength (UV, blue and red) system, in which the two competing factors, N-inhibition and S-inhibition, could be independently and selectively tailored to achieve: (i) high conversion of blue-light (without UV-light), enhanced by red-light pre-irradiation for minimal S-inhibition; and (ii) efficient PC initiated by UV-light which produces N-inhibition for reduced confinement thickness and for high print speed.

For the first time, this article will present the detailed kinetics for a 3-wavelength PC system. Analytical solutions for the kinetic equations and formulas will be derived. Then, we will show the numerical results for the oxygen, free radical and conversion profiles for blue-light only, 2-light (red and UV), and 3-light (red, blue, UV) situations. The role of oxygen, N- and S-inhibition are explored. We will discuss the inhibition-depth and strategy for accelerated printing speed, and the criterion for an efficient PC, which is governed by multiple factors. Finally, the theory (formulas) developed in this study could be further explored/justified by suggested experiments, which are the extension of the dual-wavelength systems reported by de Beer *et al.* [9], van der Laan *et al.* [10] and Lin [14].

This paper is organized as follows. The materials and methods are introduced in section 2. The results are issued in section 3. Finally we make a conclusion in section 4.

II. MATERIALS AND METHODS

A. PHOTOCHEMICAL KINETIC

As shown by Fig. 1, a 3-wavelength (red, blue and UV light) radical-mediated system consists of 4 photoinitiators, A, B, C and D (as a donor). The blue-light conversion of monomer [M] could be enhanced by pre-irradiation of a red-light which reduces the oxygen-inhibition. On the other hand, the conversion could be reduced by the UV-light produced inhibitor [N], as a switch-off mechanism for controlled spatial confirmation.

The initiation radicals R and [X] initiate the monomer [M] photopolymerization; whereas the inhibition radical [N] reduces the radical R, and thus the conversion efficacy. Also shown is the co-initiator (D) which reacts with the triplet state of A (A^*) forming an intermediate radical (R'), and a propagating radical (R) initiating crosslinks. Terminations could be resulted by the interaction among R', R, and [N], and the bimolecular recombination of R' and R.

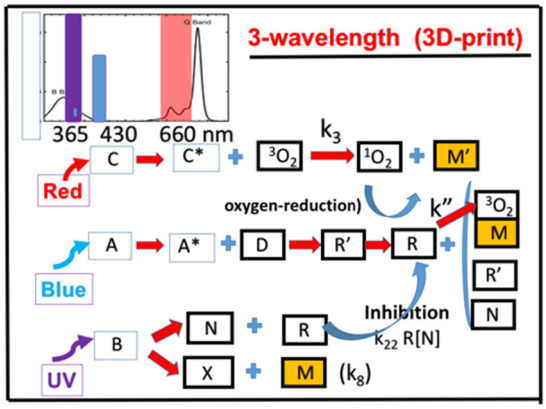

FIGURE 1. Schematics of photochemical pathways of a 3-wavelength photopolymerization, in which crosslinkers are formed via three pathways: the photoinitiator A (under a blue light), B (under a UV light), and oxygen-mediated C (under a red light). The initiation radicals R, [1O2] and [X] initiate the monomer [M] polymerization; whereas the inhibition radical [N] reduces the active radical R. Also shown is the co-initiator (D) which reacts with the triplet state of A (A∗) forming an intermediate radical (R′) and a reactive radical (R), initiating crosslinkers; terminations may be resulted by the interaction among R′, R and [N]. The blue-light conversion could be enhanced by pre-irradiation of the red-light which reduces the oxygen-inhibition effect; whereas it could be reduced by the inhibitor [N], as a switch-off mechanism. Right hand side shows the couplings among R and (R′, N, M, 3O2), in which the oxygen inhibition is governed by the rate constant, k″.

Example of blue and UV dual-wavelength system (without the red-light) for enhanced conversion by reducing the oxygen inhibition was reported by de Beer *et al.* [9] and van der Laan *et al.* [10], in which a blue (470 nm) and a UV (365 nm) light were used for the photopolymerization of methacrylate formulated with camphorquinone (CQ) and ethyl 4-(dimethylamino)benzoate (EDAB), where CQ is the blue-light active initiator (A), butyl nitrite (BN) is the UV-activated initiator (B), and EDAB is a co-initiator (or donor D). The photochemical decomposition of BN results in the formation of nitric oxide (N), an efficient inhibitor of radical-mediated polymerizations, and alkoxide radical (X) for extra polymerization initiation, besides the initiation radical (R) generated from the blue-light (to be discussed as follows).

Example of 2-wavelength (red and UV) system (without the blue-light) for PC was reported by Childress *et al.* [11], in which a monomer of ethyl ether acrylate (DEGEEA) mixed by zinc 2,9,16,23-tetra-tert-butyl-29H,31H-phthalocyanine (ZnTTP) as an initiator under a UV-light, where ZnTTP/DEGEEA has distinct absorption peak at UV-365 nm and red-635 nm, respectively, and thus it can be independently excited by a UV and a red light, respectively.

From the above two examples, one might have the option of using one single UV-light as an initiation of ZnTTP and also to produce an inhibitor (N), such that only a dual-wavelength (red and UV) is needed for the dual-function of enhancement and confinement. However, the simultaneously irradiation of UV-light for initiation and inhibition has the drawback of losing the advantage offered by a 3-wavelength system, in which each of the 3-color could be turned on and off, sequentially and independently for both spatial and temporal control which could not be achieved by 2-wavelength.

Our red-blue-UV system could be extended to the following as far as these 3 wavelengths have minimal overlap in their absorbance spectra, such as: (i) red-light (635 nm), green (532 nm), and UV-A (365 nm); (ii) near-IR (750-810 nm), red (630-660 nm), and near UV (365-405 nm); where most of these lights are available from the output of LED, and the associated photosensitizers (or photoinitiator).

Short-hand notations for the concentration of various components are used: [A], [B],[C], [D] for the ground state concentration of A, B, C, D, respectively; [O2], [Y] and [X] for the concentration of ground state oxygen, singlet oxygen radical, and inhibitor radical, respectively, and [M'] and [M] are monomers. The kinetic equations for the 3-wavelength and 5 radicals (R',R, [N], [X], [Y]) system are derived, based on the schematics of Figure 1, as follows

$$\frac{\partial[A]}{\partial t} = -gB_1\,[D]\,[A] \tag{1}$$

$$\frac{\partial[B]}{\partial t} = -g'B_2\,[M]\,[B] \tag{2}$$

$$\frac{\partial[C]}{\partial t} = -g''g_3[C]B_3[O_2][C] \tag{3}$$

$$\frac{\partial[D]}{\partial t} = -gB_1\,[D]\,[A] + R_E \tag{4}$$

$$\frac{\partial[O_2]}{\partial t} = -\left(g''B_3[C] + k''R\right)[O_2] + P \tag{5}$$

$$\frac{\partial[N]}{\partial t} = B_2\,[B] - k_{22}R[N] \tag{6}$$

$$\frac{\partial[X]}{\partial t} = B_2\,[B]\,(k_6 + k_8\,[M]\,)[X] \tag{7}$$

$$\frac{\partial R'}{\partial t} = gB_1\,[D]\,[A]\,(2k_TR' + k_{12}R)R' \tag{8}$$

$$\frac{\partial R}{\partial t} = 2k_TR'^2 - 2k_TR^2 - \left(k'\,[M] + k_{12}R' + k''[O_2] + k_{22}\,[N]\right)R \tag{9}$$

$$\frac{\partial[M]}{\partial t} = -(k_8\,[X] + g''g_3B_3[C][O_2] + k'R)[M] \tag{10}$$

where $B_1 = b_1I_1(z,t)$, $B_2 = b_2I_2(z,t)I_3(z,t)/I_{30}$, $B_3 = (b_3/b_2)B_2$; $g=1/(k_{57}+[D])$; $g'=1/(k_{68}+[M])$, $g''=1/(k_{63}+k''[O_2])$, $g_3 = 1/(k_{63}+k_{13}[C]+k_{83}[M'])$; where $k_{ij} = (k_i/k_j)$. R_E is the [D] regeneration term given by $R_E = k''R[O_2]+k_{22}[N]R+2k_TR^2$. $b_j = 83.6a_jq_jw_j$; a_j is the extinction coefficient for A, B and C (with j=1,2,3); the light wavelength (in cm), w_1 for the blue (at 470 nm), w_2 for UV (at 365 nm), w_3 for red (at 635 nm) and light intensity $I_j(z,t)$ in mW/cm^2; q_j is the quantum yields of the [A] triplet state and PB radical [12], [14].

All the reaction rate constants are defined by the associated coupling terms. For examples, in Eq. (7), k' is for the reaction of monomer and radical R, which has a relaxation rate k5; k12 is for the radical interaction of R' and R, and both have a bimolecular termination rate of kT. More detailed derivation and definition of rate constants in g and g' have been previously published [12], [15].

Using the quasi-steady-state conditions of [12] d[N]/dt= d[X]/dt=d[R']/dt=0, we obtain steady-state radicals given by [N]=B2[B]/(k22R), [X]=g'B2[B]/k8. For analytic solutions, we consider the situation that k57≪[D],, k68≪[M], k63≪k''[O2],(k63+M)≪k13[C]), such that g[D]=g'[M] =g3[C]= g''[O2]=1; and Eq. (1) to (10) are simplified to

$$\frac{\partial[\mathrm{A}]}{\partial \mathrm{t}} = -\mathrm{B}_1\,[\mathrm{A}] \tag{11}$$
$$\frac{\partial[\mathrm{B}]}{\partial \mathrm{t}} = -\mathrm{B}_2[\mathrm{B}] \tag{12}$$
$$\frac{\partial[\mathrm{C}]}{\partial \mathrm{t}} = -\mathrm{B}_3\,[\mathrm{C}] \tag{13}$$
$$\frac{\partial[O_2]}{\partial \mathrm{t}} = -B_3\,[\mathrm{C}] - \mathrm{k}''\mathrm{R}[O_2] + \mathrm{P} \tag{14}$$
$$\frac{\partial[\mathrm{M}]}{\partial \mathrm{t}} = -\mathrm{R}_\mathrm{T}\,[\mathrm{M}] \tag{15}$$
$$\mathrm{R}_\mathrm{T} = \mathrm{B}_2\,[\mathrm{B}] + \mathrm{B}_3\,[\mathrm{C}] + \mathrm{k}'\mathrm{R} \tag{16}$$

where R_T is a total rate constant which consists of three crosslink components attributed from the radicals [X], singlet-oxygen, and free radical (R). Furthermore, the steady-state radicals, R' and R, are given by, where we keep the g[D] term for more general case,

$$2\mathrm{k}_\mathrm{T}\mathrm{R}'^2 + \mathrm{k}_{12}\mathrm{R}' - \mathrm{g}[\mathrm{D}]\mathrm{B}_1\,[\mathrm{A}] = 0 \tag{17}$$
$$2\mathrm{k}_\mathrm{T}\mathrm{R}^2 + \left(k'\,[\mathrm{M}] + \mathrm{k}''[O_2] + \mathrm{k}_{12}\mathrm{R}'\right)\mathrm{R} - (2\mathrm{k}_\mathrm{T}\mathrm{R}'2 - \mathrm{B}_2\,[\mathrm{B}]) = 0 \tag{18}$$

Solving for Eq. (11) and (12), we obtain [15]

$$R = \left(\frac{1}{4\mathrm{k}_\mathrm{T}}\right)[-G + \sqrt{G^2 + 8\mathrm{k}_\mathrm{T}\mathrm{H}}] \tag{19}$$
$$\mathrm{H} = \mathrm{g}[\mathrm{D}]\mathrm{B}_1\,[\mathrm{A}] - \mathrm{B}_2\,[\mathrm{B}] \tag{20}$$

where G=k'[M]+k''[O_2]+2k_{12}R'. Eq. (19) may be further approximated to R=$(0.5\mathrm{H}/\mathrm{k}_\mathrm{T})^{0.5}$ −(k'[M]+k''[O_2]) (1-d), with d=$0.5\mathrm{G}^2/(8\mathrm{k}_\mathrm{T}\mathrm{H})$, for $2\mathrm{k}_{12}\mathrm{R}' \ll \mathrm{k}'[\mathrm{M}]$, which shows that R and efficacy are increasing function of H. The balance point of inhibition depth is defined by when R=0, or $8\mathrm{k}_\mathrm{T}\mathrm{H}=0$, or $\mathrm{B}_1[\mathrm{A}]=\mathrm{B}_2[\mathrm{B}]$, for g[D]=1, in which the [A] initiated radical (R) is completely inhibited/consumed by the [B] radical, [N], and thus the total rate function R_T of Eq. (16) is by the first two terms, $\mathrm{B}_2[\mathrm{B}]+\mathrm{B}_3[\mathrm{C}]$. We will have more discussion later.

The dynamic light intensity of blue (I_1) and UV (I_2) are given by, when they are applied to the resin orthogonally and separately [13], [15], [16]

$$I_j\,(z,t) = I_{j0}\exp\left[-A_j z\right] \tag{21}$$
$$A_j\,(\mathrm{z},\mathrm{t}) = 2.3(a_j C_{j0} + Q_j) - A_{j1}\mathrm{t} \tag{22}$$

where a_j is the extinction coefficients of [A] (for j=1) and [B] (for j=2) and their photolysis products, respectively; Q_j is the absorption coefficient of the monomer at the blue and UV wavelength [13]. Most previous modeling [7]–[12] assumed a constant C (z, t) in Eq. (2.b). Our analytic formulas in this article will use a time-average of A (z, t) to count for the dynamic of light intensity due to PA and PB depletions. Accurate solutions of Eq. (1) and (8) require numerical simulations (to be shown later). For analytic formulas, we will use approximated analytic formulas for the light intensity and the PI and PE concentration and the expressive closed forms of $I_j(z,t)$ and $C_j(z,t)$ allow us to solve for the first-order and second-order solutions of R, [M] and the conversion efficacy.

B. ANALYTIC FORMULAS FOR EFFICACY

The monomer conversion efficacy for a bimolecular termination process is given by C_{EFF} = 1-[M]/$[M]_0$ = 1-exp(-S), with $[M]_0$ being the initial monomer concentration, and the S-function is given by the time integral of the total rate factor R_T given by Eq. (16). Solutions of Eq. (11) to (15) are available by the approximated analytic formulas for $I_j(z,t)$ and $C_j(z,t)$, with j=1,2,3, for [A], [B] and [C], as follow [12], [14]

$$I_j\,(z,t) = I_{j0}\,\exp\left[-A_j z\right] \tag{23}$$
$$[\mathrm{A}]\,(z,t) = [A]_0\,\exp\left[-B'_j t\right] \tag{24}$$
$$[\mathrm{B}]\,(z,t) = [B]_0\,\exp\left[-B'_j t\right] \tag{25}$$
$$[\mathrm{C}]\,(z,t) = [C]_0\,\exp\left[-B'_j t\right] \tag{26}$$

where $\mathrm{B'}_j = \mathrm{b}_j\mathrm{I}_{j0}\exp(-\mathrm{A}_j\mathrm{'z})$, $\mathrm{A}_{j1} = 2.3(\mathrm{a}_j - \mathrm{b'}_j)\mathrm{C}_{j0}\mathrm{I}_{j0}\mathrm{b}_j\mathrm{z}$, with A_j' being the time-averaged absorption given by $\mathrm{Aj'}=1.15(\mathrm{a}_j+\mathrm{b'}_j) + 2.3\mathrm{Q}_j$, and bj' the extinction coefficient of the photolysis products. We note that the $-\mathrm{A}_{j1}\mathrm{t}$ term represents the decrease of A_j', or increase of light intensity due to concentration depletions of [A], [B] and [C].

Using Eq. (25) to (28) and Eq. (11) for the total rate faction, R_T, we solve for Eq. (15) to obtain the conversion efficacy given by C_{EFF} = 1−[M]/$[M]_0$ = 1−exp(-S), with S is the time integral of R_T, which requires a numerical integration, in general. For analytic solutions, two cases are considered. For $\mathrm{gB}_j\mathrm{C}_j \ll \mathrm{k'R}$, case (i) H≫G, $\mathrm{k'R}=\mathrm{KH}^{0.5}$, with $\mathrm{K}=0.5\mathrm{k'}/\mathrm{k}_\mathrm{T}^{0.5}$; case (ii) H≪G, $\mathrm{k'R}=\mathrm{KH}^{0.5}/\mathrm{G}$; where $\mathrm{H}^{0.5}$may be further reduced to $\mathrm{H}^{0.5} = (\mathrm{B}_1[\mathrm{A}])^{0.5} - 0.5(\mathrm{B}_2[\mathrm{B}])/(\mathrm{B}_1[\mathrm{A}])^{0.5}$, for $(\mathrm{B}_2[\mathrm{B}]) \ll (\mathrm{B}_1[\mathrm{A}])$, and g[C]=1, for $\mathrm{k}=\mathrm{k}_3/\mathrm{k}_7 = 1$.

In case (i), C_{EFF} = 1−[M]/$[M]_0$ = 1−exp(-S), where S-function is given by

$$S = S_1 + S_2 + S_3 \tag{27}$$
$$S_1 = D_{20}\,E_{11} \tag{28}$$
$$S_3 = D_{30}\,E_{33} \tag{29}$$
$$S_2 = K\sqrt{D_{10}}\,[E_{11} - 0.5(D_{20}/D_{10})E_{12}] \tag{30}$$
$$E_{11} = [1 - \exp(-G_{32}t)]/G_{32} \tag{31}$$
$$E_{33} = [1 - \exp(-G_{33}t)]/G_{33} \tag{32}$$
$$E_{21} = [1 - \exp(-G_{31}t)]/G_{31} \tag{33}$$
$$E_{22} = [1 - \exp[-(G_{32} - G_{31})t]/(G_{32} - G_{31}) \tag{34}$$

where initial values $\mathrm{D}_{j0} = \mathrm{B}_{j0}\mathrm{X}_j$, $\mathrm{G}_{3j} = 0.5(\mathrm{B}_{j0} - \mathrm{A}'_{1j})$, with $\mathrm{B}_{j0} = \mathrm{b}_j\mathrm{I}_{j0}\mathrm{C}_{j0}$, $\mathrm{X}_j = \exp(-\mathrm{A'}_j\mathrm{z})$, $\mathrm{A'}_j = 1.15(\mathrm{a}_j + b_j)\,\mathrm{C}_{j0} + 2.3\mathrm{Q}_j$, being a mean value of $\mathrm{A}_j(z,t)$, we have re-defined C_j with j=1,2,3 for [A], [B], [C].

For case (ii), and for k'[M]≪k'R, k'R=K'H/[M], K'=0.5/$k_T^{0.5}$, Eq. (15) becomes

$$\frac{\partial[M]}{\partial t} = -K'H(t) \tag{35}$$

Therefore, the efficacy $C_{EFF} = 1-[M]/[M]_0$ is given by the time integral of H(t)/$[M]_0$, or

$$C_{EFF} = K'S/[M]_0 \tag{36}$$

with S given by Eq. (29).

The steady-state of Eq. (28) and (29) are given by when $E_{11} = 1/G_{31}$, $E_{12} = 1/(G_{32} - G_{31})$, whereas transient-state is given by $E_{11} = E_{12} = t$. Therefore, the inhibition effect given by the second term of Eq. (32) is proportional to $B_{20}/(B_{10})^{0.5}/(G_{32} - G_{31})$, with $B_{j0} = b_j I_{j0} C_{j0}$, for steady-state; and $[tB_{20}/(B_{10})^{0.5}]$ for transient state. Numerical data will be shown later. We also note that for a given B_1C_1, the radical R is a decreasing function of the ratio of $R_{AB} = (B_2C_2)/(B_1C_1)^{0.5}$. Therefore, same R_{AB} reaches the same efficacy.

We also note that the total rate function of Eq. (16) may be further expressed as

$$R_T = G_1 - G_2 \tag{37}$$

$$G_1 = g[D]B_1[A] + B_3[C] \tag{38}$$

$$G_2 = (K-1)]B_2[B] + k'(k'[M] + k''[O_2] \tag{39}$$

which shows the following features: (i) R_T is an increasing function of G_1, or $B_1[A]$ and $B_3[C]$; but decreasing function of G_2, or $B_2[B]$ and k''$[O_2]$; (ii) for significant confirmation, one requires a small $R_T = G_1 - G_2$, or the significant reduction of conversion reduction by the coinitiator [B], or the presence of oxygen $[O_2]$; (iii) as a good switcher, one also requires reduced oxygen inhibition via [C], (when [B] is absent) for high conversion, but large [B] for a low conversion. Above features will be numerically shown later.

C. THE INHIBITION DEPTH

Polymerization inhibition depth (z_H) adjacent to the projection window is a critical parameter for continuous stereolithographic fabrication [9]–[11]. z_H defines the vertical distance into the resin from the transparent window in which no polymerization occurs. This may be calculated by the balance point of initiation and inhibition rate, or when R = 0, or H = 0. From Equation (20) and (21), we obtain [16]

$$z_H = \frac{1}{A_2 - A_1}\ln\left(\frac{B_{20}[B]_0}{gB_{10}[A]_0D_0}\right), \tag{40}$$

where $B_{j0} = b_j I_{j0}$. We note that Equation (42) defines an inhibition coefficient defined by $\beta = (b_2/b_1)[B]_0/(g[A]_0D_0)$, which depends on a multifactor and rate constants related by $g = 1/(k_{57} + k[C])$. Our formula is more general than that of de Beer *et al.* [9], which is our special case when $[B]_0 = g[A]_0D_0$, such that Equation (25) reduces to Equation (1) of de Beer *et al.* [9]: $z_H = (1/(A_2 - A_1)\ln[\beta I_{20}/I_{10}]$, with $\beta = b_2/b_1$. We note that $b_j = 83.6a_jq_jw_j$, which is defined by the extinction coefficient for A, B and D (with j = 1,2,3), by the light wavelength, w_1 for the blue (at 470 nm) and w_2 for UV (at 365 nm), and by the quantum yields (q_j). Moreover, in our more general formula, β is also proportional to $1/g = k_{57} + k[C]$, defined by the rate constants of k_{57} and $k = k_3/_7$.

A minimum intensity ratio of UV and blue light, $Rmin = (I_{20}/I_{10})_{crit}$ defined by when initiation and inhibition rates are balanced to generate an inhibition depth, $z_H = 0$ in Equation (42), and can be calculated by when $Rmin = 1/\beta' = g[A]_0D_0/[(b_2/b_1)[B]_0]$, which is dependent on resin composition ratios and rate constants. de Beer *et al.* reported $\beta' = 1$, in a TMPTA-based system [9].

D. THE PRINT SPEED

Based on Equation (22), the maximum print speed (Smax) as defined by de Beer *et al.* [9], when the dose difference of blue light and UV light equals to a critical value (E^*), and $B_1 = \beta B_2$, we obtain a similar formula:

$$S_{max} = [I_{10}/[A]_0 - \beta' I_{20}/[B]_0]/((b_1E^*) \tag{41}$$

which, however, has a more complex function $\beta' = [B]_0/(g[A]_0D_0)$, than the simplified function of de Beer *et al.* [9], with $\beta = b_2/b_1$.

Previously reported inhibition layers resulting from oxygen inhibition are typically only tens of micrometers thick. Therefore, its applications are limited to low-viscosity resins or fabrication of objects with small cross sections. In the dual-wavelength system, high rates are achievable by adjusted inhibiting (UV) intensity to maintain a constant inhibition depth. As shown by Eq. (41), high print speed requires a small $\beta' I_{20}/[B]_0$, or small z_H, by decreasing $\beta I_{20}/I_{10}$, as shown by Eq. (40).

E. THE CURING SPEED

The curing depth of the blue-light is defined by when the blue light dose, $I_{10}t$, is larger than a threshold value of E_{TH}. Using the time integral of Equation (23) with neglected A_1t, we obtain [15]

$$z_C = \frac{1}{A_1}ln\left(\frac{I_{10}t}{E_{TH}}\right) \tag{42}$$

III. RESULTS

Numerical results based on Eq. (11) to (20) are shown as follows. We will first show the conversion of blue-light only, 2-light (red and UV), and 3-light (red, blue, UV). We will explore the role of oxygen and the role of the inhibitor concentration [B]. Finally, we show the role of red-initiator [C], in the presence of both blue and UV light. For comprehensive analysis, we define two types of inhibitions which reduce the free radical (R) and conversion: (i) the co-initiator(B) and UV-light induced N-inhibition (due to the [N] radical); and (ii) the oxygen-mediated singlet-oxygen-inhibition, S-inhibition. An effective photopolymerization confinement (PC) requires a strong N-inhibition (for a low conversion), but a weak S-inhibition (for a high conversion).

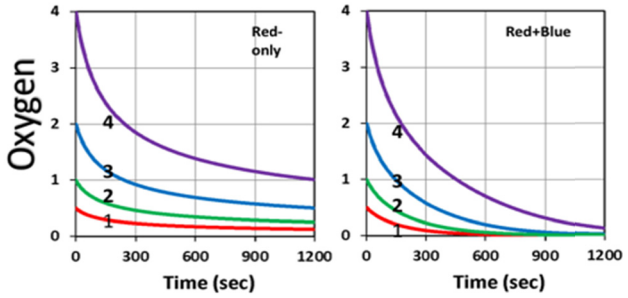

FIGURE 2. Oxygen profiles under the irradiation of red-light only (left); blue and red light (right); but in the absence of UV-light (or $B_2 = 0$), for various initial oxygen concentration of $[O_2]_0$ =(0.5,1.0, 2.0, 4.0)%, for curve (1,2,3,4); and $[A]_0$ =$[B]_0$ = 1%; B_1 =B_3 = 0.05(1/s/%); and rate constants (k,k′,k″,k_T) =(8,1, 0.1,0.5) ((1/s). profiles of blue-light (without UV-light) for (left Figure) C_{10} = (0.05, 0.1, 0.2, 0.4) %, for curve (1,2,3,4), for fixed b_1 = 0.1; and (right Figure) b_1 = (0.015, 0.05, 0.15, 0.5), for fixed C_{10} = 0.2 %; for C_{30} = 0.5 %, $[M]_0$ = 0.2%, k′ = 1.0, k_T = 0.5, k_{57} = (k_5/k_7) = k_{68} = (k_6/k_8) = k″ = 35 (1/s).

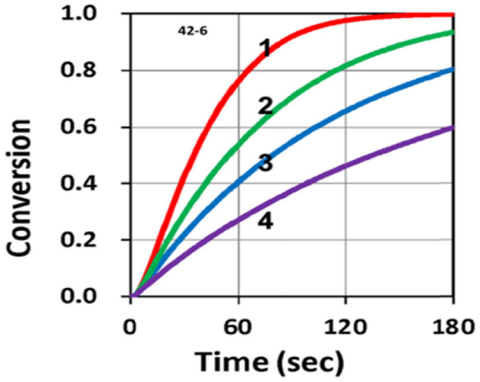

FIGURE 3. Conversion profiles under irradiation of blue-light only (with B_2 =B_3 =0), for various initial oxygen concentration of $[O_2]_0$ =(0,1.0,2.0, 4.0)mg/L, for curve (1,2,3,4).

Figure 2 shows the oxygen profiles under the irradiation of (i) red-light only, and (ii) blue and red light, in the absence of UV-light (or $B_2 = 0$), for various initial oxygen concentration of $[O_2]_0$, where oxygen depletion under a red-light only is accelerated by the blue and red-light. Figure 2 can be used to find a pre-irradiation time (T_P) to improve the conversion. For example, given an initial oxygen concentration of 2 mg/L, to obtain a reduced concentration of 1.0 mg/L and 0.5 mg/L, one requires T_R = 200 and 900 s, respectively, when only red-light is used (left Figure); however, one requires T_R reduction to 150 and 320 s, respectively, when both red and blue-light are used (right Figure).

Figure 3 shows the role of oxygen on the conversion profiles under the irradiation of blue-light only, in which conversion is a decreasing function of oxygen due to the S-inhibition. Conversion is saturated when oxygen is completely depleted. Therefore, higher initial oxygen leads to larger S-inhibition, or reduction of the free radical (R), leading to a lower conversion, as also predicted by Eq. (27).

Figure 4 shows the role of co-initiator (B) on the conversion profiles and H-function, where higher concentration, $[B]_0$, produces more inhibitor [N], or a strong N-inhibition, thus leads to a lower conversion. However, there is a transition/

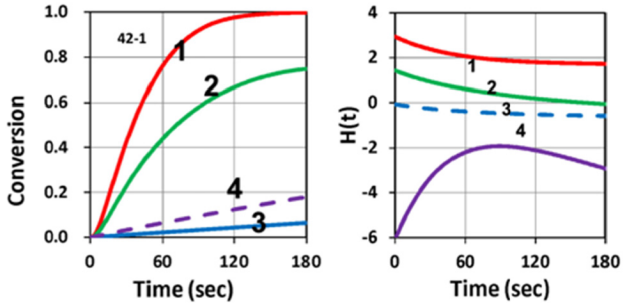

FIGURE 4. Conversion profiles (left) and H-function (right), under the irradiation of 2-light (blue and UV), without oxygen ([O2]0. =0) or the red-light (B_3 =0), for various initial concentration of $[B]_0$ =(0, 0.5, 1.0, 3.0)1%, for curves (1,2,3,4); and for (B_1, B_2) =(0.05, 0.003), and $[A]_0$ =1%.

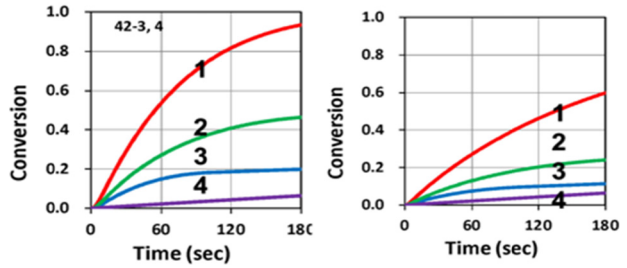

FIGURE 5. Same as figure 4, but for $[B]_0$ =(0, 0.5,0.7,1.0)1%, for curves (1,2,3,4); for $[O_2]_0$. =1.0 mg/l (left figure) and $[O_2]_0$ = 4.0 mg/l (right figure).

reversion point when H=0, (or $[B]_0$ = 1.2), i.e., reverse feature (as shown by the dashed-curve) is found that higher $[B]_0$ leads to higher conversion, resulted from the first term of the total rate R_T, as predicted by our analytic formula, Eq. (16), (19) and (37). This is one of the new findings of this modeling study, which, however, requires further experimental justification.

Figure 5 shows that the conversion is a deceasing function of the oxygen and the co-initiator concentration, $[B]_0$, or the inhibitor [N]. For an effective confinement, one requires a strong N-inhibition (or a high $[B]_0$), but also a weak S-inhibition (or a low $[O_2]_0$). Figure 5 demonstrates that higher $[O_2]_0$ has a less effective confinement. Therefore, a red-light pre-irradiation to reduce the S-inhibition is required, specially for the case of thin polymers having strong oxygen diffusion.

Figure 6 shows the conversion profiles under various irradiation conditions, where the UV-only leads to the lowest conversion, lower than the blue-only, but could be enhanced by the blue-and-UV light. Similar features are found for the oxygen profiles which are also shown by Figure 6.

Figure 7 shows the conversion profiles, under 2-light (blue and red) and 3-light (blue, red and UV), in the presence of oxygen, where significant drop of conversion (required condition for an efficient PC) occurs in the presence of UV-light (or 3-light case) and a high N-inhibition concentration, $[B]_0$. Figure 7 also shows that without the UV-light, the conversions are rather high for all ranges of oxygen, and they are a poor PC.

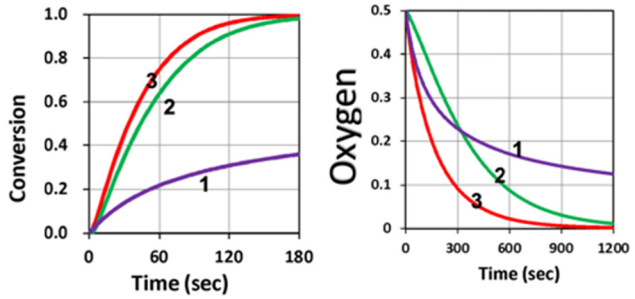

FIGURE 6. Conversion profiles (left) and oxygen concentration (right), under irradiation of UV-only (curve-1), blue-only (curve-2), and both UV and blue (curve-3); for a fixed $[O_2]_0 = 0.5$ mg/L.

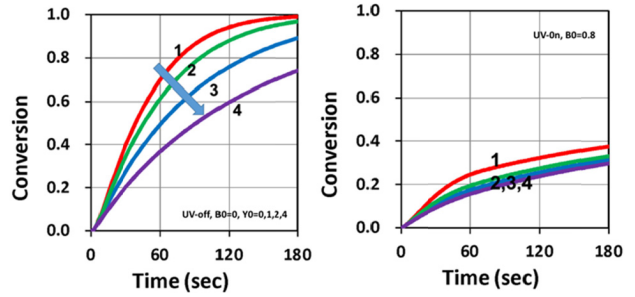

FIGURE 7. Conversion profiles under the irradiation of: (left) 2-light (blue and red); and (right) 3-light (blue, red and UV), for various initial oxygen concentration of $[O_2]_0 = (0, 1.0, 2.0, 4.0)$mg/L, for curve (1,2,3,4); with $[A]_0 = 1\%$, $[B]_0 = 0.8\%$, $[C]_0 = 1\%$.

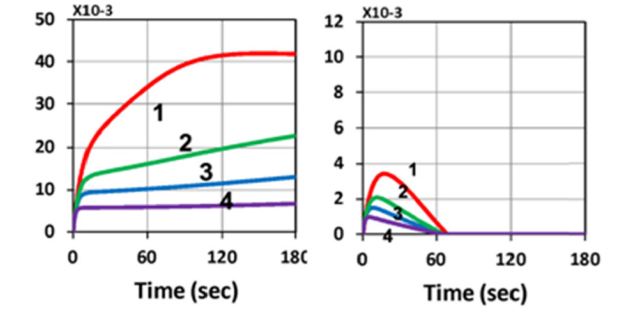

FIGURE 8. Free radical profiles under the irradiation of: (left) 2-light (blue and red); and (right) 3-light (blue, red and UV), for various initial oxygen concentration of $[O_2]_0 = (0, 1.0, 2.0, 4.0)$mg/L, for curve (1,2,3,4); with $[A]_0 = 1\%$, $[B]_0 = 0.8\%$, $[C]_0 = 1\%$.

Figure 8 shows the free radical profiles (R) associate with Figure 7, for 2-light (without UV); and 3-light (with UV), where the time integral of the R-profile gives the conversion due to blue-light induced free radical (R), as also shown by Eq. (15) and (16).

Figure 9 shows the role of the co-initiator (C), where higher concentration $[C]_0$ leads to a higher conversion due to a higher reduction of oxygen, and the S-inhibition, as also predicted by Eq. (39). Therefore, for a system having a lower conversion (in the presence of oxygen), the red-light pre-irradiation step is required in order to reduce S-inhibition.

IV. DISCUSSIONS

A. EFFICIENT UV-INHIBITION

The monomer-dependence of a dual-wavelength PC was reported by van der Laan *et al.* [10], in which different

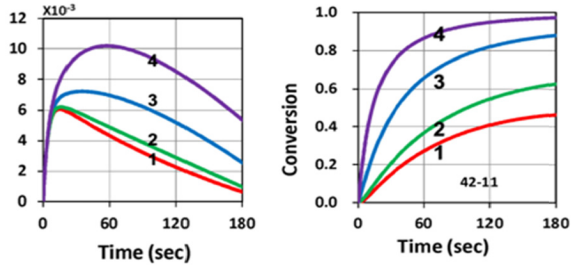

FIGURE 9. Free radical (left) and conversion profiles (right) under the irradiation of 3-light (red, blue and UV), for various initial concentration of $[C]_0 = (0, 1.0, 2.0, 3.0)1\%$, and $[A]_0 = 1.0\%$, $[B]_0 = 0.5\%$, $[O_2]_0 = 1.0\%$.

monomers have different C=C bond rate constants (K) under the exposure of blue, UV and blue+UV. For example, bisphenol ethoxylate diacrylate (BPAEDA) resins formulated with camphorquinone (CQ) and ethyl 4-(dimethylamino) benzoate (EDAB) have a maximum conversion rate constant Kmax= 0.675 s^{-1} (at blue+UV) for 0% butyl nitrite (BN), and reduces to 0.0106 s^{-1} (for 1%BN), a factor of 64 reduction. Therefore, it is a better candidate than trimethylolpropane triacrylate (TMPTA) which only has a 3 times reduction of Kmax. The above measured feature could be mathematically described by a more general criterion.

Based on our H-factor defined in Eq. (20), and shown by Figure 4 (right Figure), a general criterion for efficient UV-inhibitor, or a good PC candidate, could be mathematically determined as follows. Defining two H factors: H_{OFF} and H_{ON} for the H-value without and with UV-inhibition, respectively, then we have, H= H=$gDB_1[A]$-$B_2[B]$=H_{OFF}-H_{ON} = H_{OFF} (1-R_H), with an H-ratio, R_H =H_{ON}/H_{OFF}. Therefore, a good candidate requires two conditions: (i) a large H_{OFF} (with conversion>60%), with H_{ON} =0; and (ii) a small H (with conversion <20%, with H_{ON} > 0), i.e., R_H closes to one. For example, for a given value of $H_{OFF} = 5$, a candidate with $H_{ON} = 2$, leading to $R_H = 0.4$, and $H = 5 \times (1 - 0.4) = 3.0$, is not as good as a candidate having a higher $H_{ON} = 4$, leading to R_H =0.8 and H=1.0, which is 4 times lower, presenting a strong inhibition (or more effective PC) after the UV-light.

In the H-ratio, $R_H = B_2[B]/(gDB_1[A])$, we note that $B_j = b_j I_j$, which is proportional to the light intensities (I_1 for blue-light and and I_2 for UV-light) and the effective absorption constant (b_j) governed by the quantum yield (q) and absorption coefficient at a specific wavelength. Therefore, the H-ratio (R_H) is determined not only by the material properties, but also the ratio of light intensity (UV/blue), and concentration ratio of the initiator and inhibitor, C_{20}/C_{10}. In addition, it is also rate-constant (or monomer) dependence, because the g-factor is given by g= g=$1/(k_{57}+kC_3)$. Therefore, we conclude that the criterion for a good candidate is governed by collective factors, and at least by the double ratio of $[I_{20}C_{20}]/[I_{10}C_{10}]$. Above criterion is an important new finding of our theoretical study, which requires further experimental study to confirm.

B. DISCUSSION OF GENERAL FEATURES

From the numerical results and our analytic formulas, we are able to summarize the following important features and new findings.

(I) An effective PC requires two conditions: (i) a strong N-inhibition for uncured regime with a low conversion (triggered by the UV-light); and (ii) a weak S-inhibition (oxygen-induced) for high conversion under the blue-light or blue and red-light initiation. As shown by Figure 4, the N-inhibition is an increasing function of the inhibitor concentration, [B]. However, it is also limited by a transition value defined by H=0, which leads to R=0, as shown by Eq. (19).

(II) A reverse feature (as shown by the dashed-curve of Figure 4) is found when [B] is higher than the transition value, and thus leads to a higher conversion, resulted from the first term of the total rate R_T, as predicted by our analytic formula, Eq. (16), (19) and (37). This is one of the new findings of this modeling study, which, however, requires further experimental justification.

(III) Good material candidates for effective PC is governed by an H-ratio, R_H, and requires two conditions: (i) a large H_{OFF} (with conversion>60%), with $H_{ON} = 0$; and (ii) a small H (with conversion <20%, with $H_{ON} > 0$), i.e., R_H closes to one. A good candidate is governed by collective factors of: (i) the double ratio of light-intensity and initiator-concentration, $[I_{20}C_{20}]/[I_{10}C_{10}]$, (ii) monomers rate-constant; and (iii) effective absorption constants at specific wavelength and initiators. For example, ethyl 4-(dimethylamino) benzoate (EDAB) was reported to be a better candidate than trimethylolpropane triacrylate (TMPTA), which has a smaller R_H than that of EDAB [10].

(IV) As shown by Figure 2, higher oxygen concentration leads to a lower conversion, which could be enhanced by reducing the S-inhibition via a red or blue-light preirradiation based on the oxygen profiles shown by Figure 2. For example, to obtain a reduced oxygen concentration of 1.0 mg/L (form an initial value of 2.0 mg/L), the pre-irradiation time is given $T_P = 200$ s, when only red-light is used (left Figure 3), and reduced to 150 s, when both red and blue-light are used (right Figure 3).

(V) As shown by Figure 6, UV-only leads to the lowest conversion, lower than the blue-only. Conversion could be improved by the dual-light (blue and UV), and further enhanced by the preirradiation of red-light.

(VI) The role of oxygen is shown in Figure 7, where higher initial oxygen concentration $[O_2]_0$ and/or red-light sensitizer concentration of $[C]_0$ lead to a lower conversion, as also predicted by Eq. (37).

(VII) The two competing factors, N-inhibition and S-inhibition, could be independently and selectively tailored to achieve: (i) high conversion of blue-light (without UV-light), enhanced by red-light pre-irradiation for minimal S-inhibition; and (ii) efficient PC initiated by UV-light produced N-inhibition for reduced confinement thickness for high print speed.

Therefore, comparing to the 2-wavelength system, our proposed 3-wavelength system offers the advantages of being more efficient, and the two competing N-inhibition and S-inhibition could be selectively tailored, in which the dual wavelength (UV, blue), (UV, red) and (blue, red) could be independently controlled for best outcomes.

C. SUGGESTED EXPERIMENTS

In our previous modeling of a dual-wavelength system [16], we have successfully analyzed the measured results of de Beer *et al.* [9] and van der Laan *et al.* [10]. The theory (formulas) developed in this 3-wavelength system could be further explored/justified by the following suggested experiments.

(i) Our proposed double ratio $[I_{20}C_{20}]/[I_{10}C_{10}]$ criterion could be experimentally justified by an experimental setup having adjustable light intensities and the initiator concentrations. The experimental setup of Childress *et al.* [11], using various light red and UV light intensity (I_{10} and I_{20}), but fixed concentrations of $C_{10}$and C_{20}, could be easily extended for variable concentrations, such that our double ratio criterion could be justified. In addition, various materials may be used to test the monomer-dependence of our H-ratio.

(ii) The dual-wavelength setup of de Beer *et al.* [9] and van der Laan *et al.* [10] could be extended to include a third red-light to reduce the oxygen inhibition by red-light pre-irradiation, specially for thin film cases, where PC efficacy and printing speeds could be measured to justify our proposed strategies.

V. CONCLUSION

We have presented the detailed kinetics for a 3-wavelength PC system, in which both numerical solutions and analytic formulas are explored. The dynamic profiles are simulated for oxygen, free radical, and conversion for various situations of: blue-light only, 2-light (red and UV), and 3-light (red, blue, UV). An effective PC requires two conditions: (i) a strong N-inhibition for uncured regime having a low conversion (triggered by the UV-light); and (ii) a weak S-inhibition (oxygen-induced) for high conversion under the blue-light or blue and red-light initiation. Good PC candidates are governed by a criterion defined by collective factors of: (i) the double ratio of light-intensity and initiator-concentration, (ii) monomers rate-constants; and (iii) effective absorption constants at specific wavelength and initiators. Higher oxygen concentration leads to a lower conversion, which could be enhanced by reducing the S-inhibition via a red or blue-light pre-irradiation. The strategy for an efficient PC could be achieved by tailoring the two competing factors, N-inhibition

and S-inhibition, independently via the steps of: (i) red-light pre-irradiation for minimal S-inhibition (oxygen-inhibition); and (ii) followed by a combined irradiation of UV and blue light, under the criterion for efficient PC to achieve reduced confinement depth, and high print speed.

Conflict of interest: Jui-Teng Lin is the CEO of Photon Vision Corp., Taipei, Taiwan. The other authors have no conflict of interest. The funders had no role in the design of the study; in the collection, analyses, or interpretation of data; in the writing of the manuscript, or in the decision to publish the results. Author DC Cheng has received research grants from the China Medical University under grant number CMU 109-S-25.

ACKNOWLEDGMENT

(Jui-Teng Lin and Hsia-Wei Liu contributed equally to this work.) The authors are grateful to the National Center for High-performance Computing for computer time and facilities.

REFERENCES

[1] G. Gao, Y. Zhang, D. Ramanujan, and K. Ramani, "The status, challenges, and future of additive manufacturing in engineering," *Comput. Aided Des.*, vol. 69, pp. 65–89, Dec. 2015.
[2] S. C. Ligon, R. Liska, J. Stampfl, M. Gurr, and R. Mulhaupt, "Polymers for 3D printing and customized additive manufacturing," *Chem. Rev.*, vol. 117, no. 15, pp. 10212–10290, Aug. 2017.
[3] M. Shusteff, A. E. M. Browar, B. E. Kelly, J. Henriksson, T. H. Weisgraber, R. M. Panas, N. X. Fang, and C. M. Spadaccini, "One-step volumetric additive manufacturing of complex polymer structures," *Sci. Adv.*, vol. 3, no. 12, 2017, Art. no. eaao5496.
[4] Z. Li, R. Xu, Z. Zhang, and I. Kucukkoc, "The influence of scan length on fabricating thin-walled components in selective laser melting," *Int. J. Mach. Tools Manuf.*, vol. 126, pp. 1–12, Mar. 2018.
[5] M. Zhao, D. Z. Zhang, F. Liu, Z. Li, Z. Ma, and Z. Ren, "Mechanical and energy absorption characteristics of additively manufactured functionally graded sheet lattice structures with minimal surfaces," *Int. J. Mech. Sci.*, vol. 167, Feb. 2020, Art. no. 105262.
[6] H. Yi, L. Qi, J. Luo, and N. Li, "Hole-defects in soluble core assisted aluminum droplet printing: Metallurgical mechanisms and elimination methods," *Appl. Thermal Eng.*, vol. 148, pp. 1183–1193, Feb. 2019.
[7] W. Zhu, K. R. Tringale, S. A. Woller, S. You, S. Johnson, H. Shen, J. Schimelman, M. Whitney, J. Steinauer, W. Xu, T. L. Yaksh, Q. T. Nguyen, and S. Chen, "Rapid continuous 3D printing of customizable peripheral nerve guidance conduits," *Mater. Today*, vol. 21, no. 9, pp. 951–959, Nov. 2018.
[8] T. F. Scott, B. A. Kowalski, A. C. Sullivan, C. N. Bowman, and R. R. McLeod, "Two-color single-photon photoinitiation and photoinhibition for subdiffraction photolithography," *Science*, vol. 324, no. 5929, pp. 913–917, May 2009.
[9] M. P. de Beer, H. L. van der Laan, M. A. Cole, R. J. Whelan, M. A. Burns, and T. F. Scott, "Rapid, continuous additive manufacturing by volumetric polymerization inhibition patterning," *Sci. Adv.*, vol. 5, no. 1, Jan. 2019, Art. no. eaau8723.
[10] H. L. van der Laan, M. A. Burns, and T. F. Scott, "Volumetric photopolymerization confinement through dual-wavelength photoinitiation and photoinhibition," *ACS Macro Lett.*, vol. 8, pp. 899–904, Jul. 2019.
[11] K. K. Childress, K. Kim, D. J. Glugla, C. B. Musgrave, C. N. Bowman, and J. W. Stansbury, "Independent control of singlet oxygen and radical generation via irradiation of a two-color photosensitive molecule," *Macromolecules*, vol. 52, no. 13, pp. 4968–4978, Jul. 2019.
[12] J. T. Lin, "Efficacy S-formula and kinetics of oxygen-mediated (type-II) and non-oxygen-mediated (type-I) corneal cross-linking," *Ophthalmol. Res.*, vol. 8, no. 1, pp. 1–11, 2018.
[13] J.-T. Lin and D.-C. Cheng, "Modeling the efficacy profiles of UV-light activated corneal collagen crosslinking," *PLoS ONE*, vol. 12, no. 4, 2017, Art. no. e0175002.
[14] J. T. Lin, "Kinetics of enhancement for corneal cross-linking: Proposed model for a two-initiator system," *Ophthalmol. Res.*, vol. 10, no. 3, pp. 1–6, 2019.
[15] J.-T. Lin, H.-W. Liu, K.-T. Chen, and D.-C. Cheng, "Modeling the kinetics, curing depth, and efficacy of radical-mediated photopolymerization: The role of oxygen inhibition, viscosity, and dynamic light intensity," *Frontiers Chem.*, vol. 7, p. 760, Nov. 2019.
[16] J.-T. Lin, D.-C. Cheng, K.-T. Chen, and H.-W. Liu, "Dual-wavelength (UV and Blue) controlled photopolymerization confinement for 3D-printing: Modeling and analysis of measurements," *Polymers*, vol. 11, no. 11, p. 1819, 2019.
[17] J. Alvankarian and B. Y. Majlis, "Exploiting the oxygen inhibitory effect on UV curing in microfabrication: A modified lithography technique," *PLoS ONE*, vol. 10, no. 3, 2015, Art. no. e0119658.

JUI-TENG LIN received the Ph.D. degree in physics from the University of Rochester, USA, in 1981. He was a Visiting Professor with National Chao-Tung University, Taiwan, and He Medical University, China. He was an Associate Professor with the University of Central Florida, USA. He was the Founder and the CEO of Nasdaq-listed companies. He is currently the Chairman and the CEO of Photon Vision Corporation, Taiwan. He has published 55 book chapters and 250 peer-reviewed articles, in which about 100 SCI-indexed. He has over 70 international patents and was an inventor (U.S. patents, 1992 and 2000) of flying-spot LASIK procedure currently used in eye hospitals worldwide. His awards include the WHO's WHO in Leading American Executives and the Model of Oversea Chinese Young Entrepreneur. He is the Editor-in-Chief of *Open Access Journal of Ophthalmology* (OAJO) and *Journal of Ophthalmology and Research* (JOR)

HSIA-WEI LIU received the Ph.D. degree in chemical engineering from National Tsinghua University, Taiwan, in 2006. He is currently an Associate Professor with the Department of Life Science, Fu Jen Catholic University, Taiwan. His major research focuses on biomaterials and tissue engineering. His research interests include polymeric micelles drug delivery for osteoarthritis treatment, 3D bioprinting, and biological system simulation.

YIN-CHEN CHIU received the B.S. degree in mathematics and the M.S. degree in MBA. He is currently pursuing the Ph.D. degree with the Graduate Institute of Applied Science and Engineering, Fu Jen Catholic University, Taipei, Taiwan. He participates in photodynamic and photothermal therapy study of tumor, and surface coating of anti-infection and anti-calculus medical device. His main research is in the antimicrobial coating materials of intravenous cardiac catheters.

KUO-TI CHEN received the Ph.D. degree from the Graduate Institute of Applied Science and Engineering, Fu Jen Catholic University, Taipei, Taiwan, in 2020. He has more than 30 years of work experience in different engineering fields, such as biomedical, optical, electronic, and mechanical engineering. He has published more than 20 journal articles, from 2010 to 2020, including over ten SCI-indexed articles. He has developed a total of 68 new patents, including medical equipment, semiconductor packaging, as well as laser and LED applications.

DA-CHUAN CHENG received the B.S. degree in electrical engineering from Chinese Culture University, Taipei, Taiwan, in 1990, and the M.S. and Ph.D. degrees in biomedical engineering from National Cheng Kung University, Tainan, Taiwan, in 1992 and 2003, respectively.

From 1998 to 2003, he was a Research Assistant with the Department of Computer Science, Albert-Ludwigs University Freiburg, Germany. From 2004 to 2006, he held a postdoctoral position at the Department of Mathematics and Computer Science, Westfaelische Wilhelms University, Muenster, Germany. Since 2012, he has been an Associate Professor with the Department of Biomedical Imaging and Radiological Science, China Medical University, Taiwan. He has published 44 SCI-indexed journal articles. His research interests include medical image processing, computer vision, and deep learning.